Talanta 85 (2011) 1369–1375

Contents lists available at ScienceDirect

Talanta

journal homepage: www.elsevier.com/locate/talanta

Discourse on the utilization of polyaniline coatings for surface plasmon resonance sensing of ammonia vapor

Nicola Menegazzo[a], Bryon Herbert[a], Soame Banerji[b], Karl S. Booksh[a,*]

[a] University of Delaware, Department of Chemistry and Biochemistry, Newark, DE 19716, United States
[b] Arizona State University, Department of Chemistry and Biochemistry, Tempe, AZ 85287, United States

ARTICLE INFO

Article history:
Received 22 April 2011
Received in revised form 9 June 2011
Accepted 10 June 2011
Available online 17 June 2011

Keywords:
Surface plasmon resonance spectroscopy
Polyaniline camphorsulfonic acid
Ammonia
Gas-phase sensing

ABSTRACT

Surface plasmon resonance spectroscopy is sensitive to near-surface (<300 nm) chemical and physical events that result in refractive index changes. The non-specific nature of the stimulus implies that chemical selectivity in SPR sensing configurations entirely relies upon the chemical recognition scheme employed. Biosensing applications commonly use surface layers composed of antibodies or enzymes for biomolecular recognition. Monitoring of volatile compounds with SPR spectroscopy, however, has not been widely discussed due to the difficulty in selectively responding to small molecules (<100 Da) in addition to the limited refractive index changes resulting from the interaction between the plasmon wave and volatile compounds.

Different strategies explored thus far for sensing of small molecules have relied on optical and electrical changes of the recognition layer upon exposure to the analyte, yielding an indirect measurement. Examples of coatings used for gas-phase sensing with SPR include conducting metal oxides, polymers and organometallic dyes. Electrically conducting polymers, like polyaniline and polypyrrole, display dramatic conductivity changes in the presence of certain compounds. This property has resulted in their routine incorporation into different sensing schemes. However, application of electrically conducting polymers to SPR gas-phase sensing has been limited to a few examples, despite encouraging results.

The emeraldine salt form of polyaniline (PAni) demonstrates a decreased electrical conductivity correlated to NH_3 concentration. In this contribution, PAni doped with camphorsulfonic acid (PAni-CSA) was applied to gas-phase sensing of NH_3 by way of SPR spectroscopy. Spectroscopic ellipsometry was used to determine the optical constants (n and k) for emeraldine salt and emeraldine base forms of PAni, confirming the wavelength-dependent response observed via SPR. The analytical performance of the coatings show that a limit of detection of 32 ppm NH_3 based on precision of the mass-flow controllers used and an estimated method limit of detection of ~0.2 ppm based on three standard deviations of the blank. This is directly comparable to other, more established sensing architectures.

1. Introduction

Surface plasmon resonance (SPR) spectroscopy is commonly used to measure changes in the dielectric constant (ultimately, the refractive index) of a sample [1,2]. The technique relies upon optical excitation of surface plasmon polaritons (SPPs), collective charge oscillations, in thin films of appropriate materials (typically, gold, silver and copper though metal oxides have also been used) and occurring at the interface between the film and surrounding dielectric (i.e., the sample). The intensity of the plasmon wave decays exponentially yielding a penetration depth of ~300 nm into the metal-sample interface, rendering SPR spectroscopy especially sensitive towards near-surface events. In particular, it is well-suited for acquiring information about biochemical systems, including antibody–antigen binding constants, monitoring biofouling levels and epitope mapping [3,4]. Furthermore, since the signal measured with SPR spectroscopy originates from changes in refractive index, external labeling of biomolecules is unnecessary. SPR biosensing architectures have benefitted from both the high sensitivity to biomolecular binding events, yielding detection limits approaching sub-ng/mL levels, as well as the unnecessary incorporation of tags (e.g., fluorophores or gold nanoparticles), simplifying the analysis [5–8].

In contrast, SPR sensing of gas-phase compounds has largely remained unexplored due to the minute changes in refractive index imparted following surface adsorption of small (<100 Da) volatile compounds. Consequently, percent-level analyte concentrations are required in order to register significant changes in SPR spectra [9]. Furthermore, the non-specific nature of refractive index changes renders differentiation between chemical (e.g. ana-

* Corresponding author. Tel.: +1 302 831 2561; fax: +1 302 831 6335.
E-mail address: kbooksh@udel.edu (K.S. Booksh).

0039-9140/$ – see front matter © 2011 Published by Elsevier B.V.
doi:10.1016/j.talanta.2011.06.020

lyte) and physical (e.g. temperature or pressure changes) stimuli impossible. In order to overcome these limitations, a selection of materials have been coated onto plasmon supporting metals and evaluated for their ability to improve chemical selectivity as well as amplification of the response. Complexation reactions between organometallic compounds and the analyte have been evaluated as a way to impart chemical selectivity [10–12]; the reaction causes a change in the electronic distribution within the organometallic compound, altering its optical properties. Metal oxide coatings, such as TiO_2 [13], ZnO [14] and others [15,16], have also been explored in SPR gas-phase sensing configurations. In this case, surficial adsorption of electron-withdrawing or -donating compounds alters the electrical conductivity of the metal oxide [17], changing the complex permittivity (i.e. refractive index). Finally, several polymer coatings have been evaluated for their potential to enhance and discriminate the response to different gases with SPR sensors. These include polydimethylsiloxane [18], polyimide [19], Nafion [15] and polyelectrolyte multilayers [20]. The analytic signal typically stems from a physical change (i.e. swelling) of the polymer, resulting from enrichment of the analyte within the volume probed by the plasmonic wave. Chemical selectivity can be partially achieved by appropriately selecting polymers that display a preferential affinity towards the analyte (e.g. Hansen solubility parameters).

Electrically conducting polymers, such as polypyrrole and polyaniline (PAni), constitute a special class of polymer coatings commonly used in gas sensing [21–25]. The transduction principle for electrically conducting polymers relies on a change in electrical conductivity, rather than a conformational change, upon exposure to the analyte. Alternatively, optical detection based on the polymer's absorption or reflection spectral profile has also been used, albeit this approach is less popular [26]. With respect to SPR spectroscopy, application of electrically conducting polymers for chemical recognition has been limited to a few examples. Agbor et al. [27,28] demonstrated the use of Langmuir–Blodgett PAni films for H_2S and NO_2 sensing at low-ppm levels. Samoylov et al. reported on HCl sensing with a N-substituted derivative of PAni, poly(N-methylaniline), at a concentration of 80 ppm [29]. Banerji et al. [20] also employed PAni for gas sensing, albeit in the electrically insulating (pernigraniline) form as a method to test the effect of physical, rather than electronic, changes associated with NH_3 stimuli. The absence of a response to 4% NH_3 (in dry air) indicated that swelling of the recognition layer alone was not sufficient for detection of the analyte at concentrations below those tested. Furthermore, the authors postulated that the low sensitivity observed may also be related to the morphology of electropolymerized PAni, mainly constituting of loosely packed intertwined nanofibrils of up to 200 nm in diameter [30]. Since SPR spectroscopy is sensitive to RI changes occurring within 300 nm of the metal/polymer interface, the nanofibrous heterogeneity converts to diminished spectroscopically active area and in poor sensitivity.

As the conducting polymer interacts with the analyte and its electrical properties change, a concomitant change in the dielectric coefficient will be observed. Polyaniline in the emeraldine salt form displays nearly metallic conductivity, whereas it is electrically insulating in the emeraldine base form [31,32]. The latter can be partially induced by reducing compounds. Therefore, modifying SPR sensors with electrically conducting polymers has the potential to address both limitations of SPR gas-phase sensing by: (1) introducing selective chemical recognition and (2) amplifying the response, since the shift in SPR coupling conditions rises from the polymer's interaction with the analyte, rather than from the analyte directly.

Ammonia is a reducing, volatile compound commonly measured with PAni-based sensing platforms due to its well-characterized influence on the polymer's conductivity in addition to general interest for gas-phase detection [22,33,34]; NH_3 is associated with health hazards in industrial and agricultural settings [35–37]. Hence, in order to evaluate the viability of gas-phase SPR sensing, PAni doped with camphorsulfonic acid (PAni-CSA) layers were exposed to varying NH_3 concentrations in dry synthetic air. Since a shallow analytical area is probed by the plasmonic wave, PAni was deposited by drop-casting from formic acid, rather than by electropolymerization, in order to obtain continuous layers [30]. The physical properties of PAni-CSA layers used were investigated with FT-IR and UV–Vis spectroscopy confirming the presence of the emeraldine salt form. Of particular interest to sensing platforms, the wavelength-dependent optical properties of PAni-CSA are also outlined and discussed with respect to analytical performance and provide evidence that sub-ppm limits of detection may be achievable.

2. Experimental

SF-10 (Esco Products, Oak Ridge, NJ) glass slides were immersed in boiling piranha solution [3:1 (v/v) concentrated H_2SO_4:30% H_2O_2] (Fisher Scientific, Fair Lawn, NJ) for 60 min, then copiously washed with deionized water, dried with a stream of dry nitrogen gas (Keen Compressed Gas Co., Wilmington, DE) and immediately placed in a DC magnetron sputterer (model 308R, Cressington Scientific Instruments Ltd., Watford, UK). The glass slides were sputtered with 2 nm of chromium (99.95+%, Kurt J. Lesker, Clairton, PA) followed by 50 nm of gold (99.99%, Espi Metals, Ashland, OR).

Polyaniline in the emeraldine base form was prepared according to the procedure described by Sasaki et al. [38]. Briefly, PAni powder (MW ~20,000, Sigma–Aldrich, St. Louis, MO) was treated with ammonium hydroxide (Fisher Scientific, Pittsburgh, PA) to ensure full deprotonation and subsequently rinsed with deionized water. The filtrate was then dried under reduced pressure at room temperature overnight. Dry emeraldine base was dissolved in sufficient formic acid (Acros Organics, Morris Plains, NJ) to yield a 5 mg/mL stock solution. A 1 mL aliquot was pipetted out and diluted to 1 mg/mL with formic acid to which 6.4 mg of camphorsulfonic acid (Acros Organics, Morris Plains, NJ) were added resulting in a 2:1 molar ratio of acid to tetrameric PAni repeating unit. A 50 μL aliquot was drop-casted onto a gold-coated glass slide and placed in a vacuum oven at 60 °C overnight.

A drop of index-matching fluid (RI = 1.7300, Cargille Laboratories, Cedar Grove, NJ) was added to the back-side of coated slides and subsequently mounted onto SF-10 60° equilateral prisms (Esco Products, Oak Ridge, NJ). The assembly was fixed to a custom-built polycarbonate flow cell containing two channels, an analytical channel and a reference channel. Polarized collimated light from a "warm white" light emitting diode (Philips Luxeon K2, model LXK2-PWW4-U00, San Jose, CA) was guided onto the back-side of the SPR sensor and the reflected beam was steered into a grating spectrometer (Horiba Scientific, model iHR320, Edison, NJ) equipped with a TE-cooled CCD detector (Horiba Scientific, model Symphony, Edison, NJ).

Gas delivery to the analytic and reference channels was regulated by mass flow controllers (MFC, Omega, model FMA5400, Stamford, CT) operating at a flow rate of 100 mL/min. The reference channel was constantly flushed with dry synthetic air [80 nitrogen: 20 oxygen (v/v) mixture, Keen Compressed Gas Co., Wilmington, DE] whereas the analytic channel was exposed to dry ammonia vapor [0.4% (v/v) stock in synthetic air, Matheson Gas, Montgomeryville, PA] diluted with synthetic air to achieve the desired concentration. MFCs were computer-controlled using custom-written Labview virtual instruments (National Instruments, Austin,

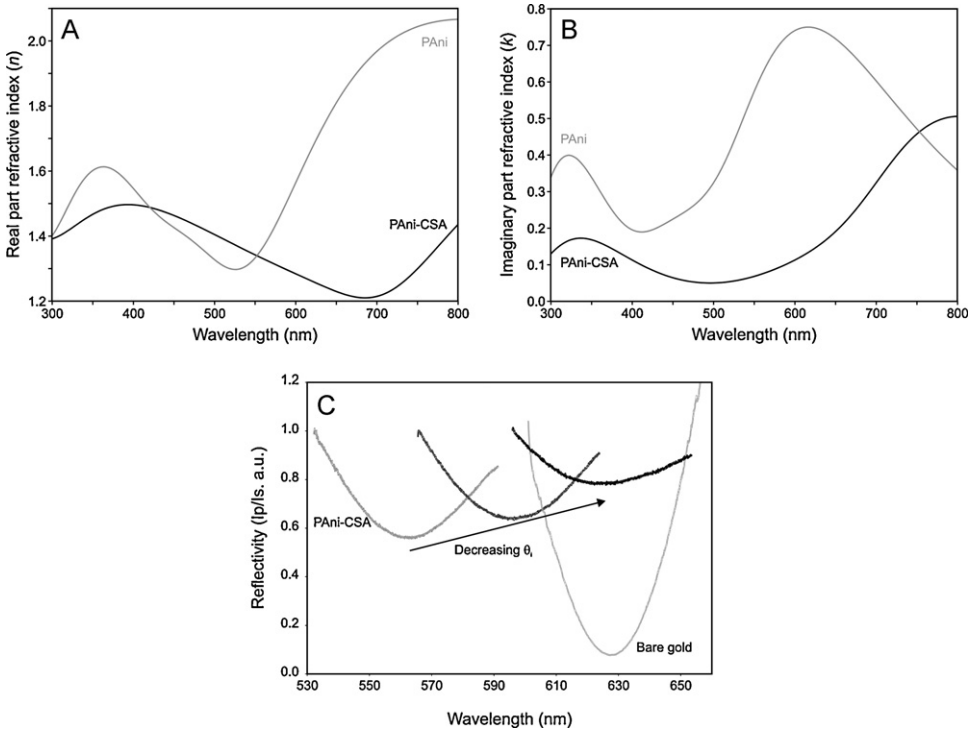

Fig. 1. (A) Real and (B) imaginary components of the refractive index for PAni (gray line) and PAni-CSA (black line). (C) SPR dips obtained with PAni-CSA at different coupling conditions compared to bare gold.

TX). Stainless steel tubing (∅ = 1/16″) and fittings were used to connect the MFCs to the flow cell.

SPR spectra collected under different polarizations (s-polarized was used as a reference) resulted from averaging of five spectra to improve signal-to-noise ratio, and were subsequently analyzed using custom-coded MATLAB routines to help identify SPR dip minima.

Reflectance FT-IR spectra of both emeraldine forms were collected as thin films drop-casted onto gold-coated glass slides in the mid-infrared range (4000–400 cm^{-1}) with a Hyperion 2000 microscope optically coupled to a Bruker Optics Vertex 70 (Billerica, MA) spectrometer. Spectra were acquired using a germanium micro-attenuated total reflectance objective (∼100 μm diameter probed spot size) and a liquid nitrogen-cooled mercury–cadmium–telluride (MCT) detector. Each spectrum consisted of 100 averaged scans at a 4 cm^{-1} resolution. PAni and PAni-CSA films drop-casted from a 50 μL aliquot of a 1 mg/mL solution onto quartz slides were utilized for spectroscopic data collection in the 190–1100 nm with a Hewlett Packard spectrophotomer (model 8453, Santa Clara, CA) with a 1 nm resolution.

Polymer thickness was measured with a Bruker AXS atomic force microscope (AFM, model Dimension 3100, Santa Barbara, CA) in tapping mode with silicon probes (BudgetSensors, model Tap300, Sofia, Bulgaria). Two glass slides were simultaneously sputtered with 50 nm of gold (without chromium); one was coated with PAni-CSA by drop-casting 50 μL of the 1 mg/mL solution. A step was created on both glass slides by adhering tape to a portion of the slides and gently peeling it off, thereby exposing the underlying glass substrate. Gold thickness was measured from bare slides and subsequently subtracted from PAni-CSA coated substrates. The resulting calculated thickness corresponds to the polymer itself. Prior to thickness measurements, micrographs were flattened with a 1st order plane fit to mathematically remove tilt in the system using software routines embedded in the software controlling the AFM. Three images were recorded for each sample and three thickness values were retrieved from each images; the thickness reported results from the average (plus standard deviation) of nine data points.

Real and imaginary components of the complex refractive index for PAni-CSA were obtained with an automated J.A. Woollam (Lincoln, NE) variable angle spectroscopic ellipsometer (VASE) covering the 250–1700 nm spectral range. SE measurements were collected at 55°, 65° and 75° and analyzed using the software package provided by the instrument manufacturer.

3. Results and discussion

3.1. Physical characterization

The presence of CSA and formation of the emeraldine salt was confirmed by FT-IR spectroscopy. PAni spectra exhibit characteristic absorption bands at 1586 cm^{-1} (N═quinoid═N), 1507 cm^{-1} (N-benzoid-N) and 1168 cm^{-1} (C–H in-plane bending). Addition of CSA introduces strong contributions at 1043 cm^{-1} ($-SO_3$) and 1742 cm^{-1} (C═O) [39] as well as a shift in absorption wavenumber of the $C{=}N^{\bullet+}$ stretching from 1270 cm^{-1} in PAni to 1236 cm^{-1} in PAni-CSA [40] and an increased absorbance at 1612 cm^{-1} (N = ring stretching) [39] (Fig. 1A SI). Absorption spectra in 300–900 nm wavelength range (Fig. 1B SI) further verify doping of PAni. Three absorption bands, consistent with a coil-like conformation [41], are observed with peak absorbances at approximately 350 nm (π-to-polaron transition), 425 nm (polaron-to-π*) and 800 nm (π-to-π* related to hyperconjugated backbone) [40,42].

Wavelength-dependent optical constants for PAni and PAni-CSA were determined by spectroscopic ellipsometry (Fig. 1). Values for the real, *n*, and imaginary, *k*, components of the refractive index obtained for PAni are consistent with those published by Mo et al. [43]. A similar direct comparison for the emeraldine salt is not possible due to the different dopants used (CSA vs. HCl), which can affect the polymer's electronic and optical properties [44]. The refractive index of spin-coated PAni-CSA was reported

by Al-Attar et al. in the visible and near-infrared range [45]. However, the values for n and k reported are not in agreement with those presented in this study. For example, Al-Attar et al. reported a parabolic behavior for n, with values ranging from ~1.465 to ~1.504 in the wavelength range studied, with the highest value measured at ~530 nm. With our samples, n decreases from ~1.497 at 400 nm to ~1.210 at 700 nm, subsequently increasing to ~1.432 at 800 nm (Fig. 1A). Additional contrast rises from k, where Al-Attar et al. describe a monotonically increasing behavior towards shorter wavelengths. The PAni-CSA samples studies herein (Fig. 1B) however show the opposite, that is, a generally decreasing trend for k from longer to shorter wavelengths. The origin of this discrepancy may lie in differences in the casting solvents used. PAni-CSA coatings deposited from formic acid solutions yield UV–Vis spectra containing the aforementioned features, coatings cast from solvents like m-cresol and 2-chlorophenol adopt an expanded coil-like conformation [41] and display very different absorption profiles with a single peak at ~440 nm and an increasing "free carrier tail" in the near-infrared region.

Considering that k is related to the extinction coefficient, α, via:

$$k = \frac{\alpha\lambda}{4\pi} \quad (1)$$

and that the Beer–Lambert law further describes the association of α to the optical absorption, it becomes evident that the trend in k reported by Al-Attar et al. follows an absorption profile comparable to PAni-CSA coatings cast from solvents that favor the expanded coil-like conformation [41], and therefore, n and k reported by Al-Attar et al. are not directly comparable to ours.

Validity of the optical constants presented can be further confirmed by deriving n from k from transmission-absorption spectra via the Kramers–Kronig relation [46], which yields values similar to those obtained experimentally with ellipsometry. The general agreement between UV–Vis spectra and spectroscopic ellipsometry indicates that the optical constants extracted for our PAni-CSA samples, and their subsequent application in sensing platforms.

PAni-CSA layers were imaged by atomic force microscopy in order to determine coating thickness. The gold (and gold-PAni-CSA) was partially removed, exposing the underlying glass slide and creating the step used to measure thicknesses. Gold and gold-PAni-CSA coatings were measured at three locations; the thickness of the bare gold coating was then subtracted from combined gold-PAni-CSA to obtain the polymer thickness. This procedure yielded values of 161 ± 10 nm for PAni-CSA. Using the complex refractive index for gold [47] and PAni-CSA (Fig. 1), the penetration depth (d_p) of the surface plasmon wave into the polymer film can be calculated [2]. It was determined that in the range of λ_{SPR} = 550–640 nm, d_p increases from ~130 nm to ~260 nm. This indicates that while the plasmon wave is fully contained within the sensing material at lower wavelengths, at longer wavelengths the gas-phase above the polymer will contribute to the λ_{SPR} shift recorded. For example, at λ_{SPR} = 640 nm the intensity of the exponentially decaying plasmon wave decreased to 54% of the intensity at the metal/PAni-CSA interface (z = 0 nm), thereby partially extending beyond the polymer. However, contributions from the gas-phase atop the polymer are not anticipated to substantially influence the sensor response, since the exponentially decaying behavior of the plasmon wave implies that the greatest sensitivity to signal changes rises from analytical volumes closer to the metal/PAni-CSA interface. Additional evidence towards the negligible contribution from NH_3 in the gas phase on the sensor response will be discussed in the following section.

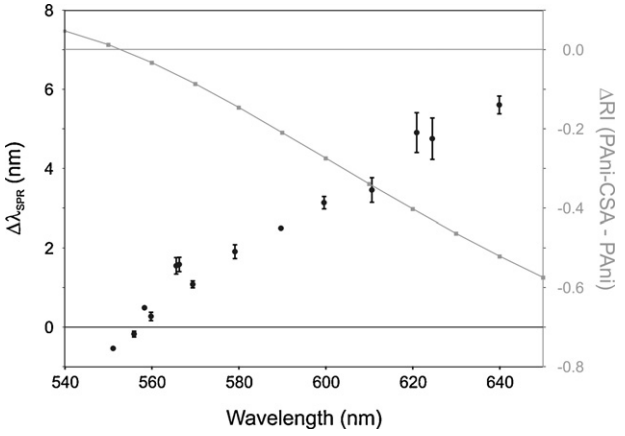

Fig. 2. λ_{SPR} shift to 192 ppm NH_3 as a function of plasmon excitation wavelength (left axis) compared to the RI difference between PAni-CSA and PAni (right axis).

3.2. Sensing characteristics

Overlapping of the plasmon resonance with absorption features pertaining to the polymer (the imaginary portion of the refractive index, k, Fig. 1B) leads to broadening of the SPR dip, as well as increased reflectivity minima (i.e., a 'shallower' dip) [48–51]. Exemplary dips as a function of coupling conditions are shown in Fig. 1C along with a dip obtained with a bare gold slide for comparison. These effects render evaluation of the dip minima (λ_{SPR}) location challenging, increasing the noise associated with uncertainties in determining the dip minima location. In order to improve the accuracy, noise levels were reduced by averaging five spectra. Averaging reduces the standard deviation of the dip location for steady-state spectra collected over 50 min from ±0.1 nm to ±0.04 nm. Increasing the averaging to ten spectra does not reduce variance levels sufficiently (±0.03 nm) to counterbalance the loss in temporal resolution: ~30 s for five spectra, compared to ~60 s for ten spectra. Therefore, for the analysis presented here, spectral averaging was maintained at five spectra per data point presented.

While the SPR dip shape is influenced by k, the dip location (i.e. λ_{SPR} and θ_{SPR}) is more directly determined by n. The wavelength dependency of n displayed by both emeraldine forms indicate that the sensing characteristics of PAni-CSA to NH_3 will vary substantially with the plasmon excitation conditions employed. That is, according to the ellipsometric data (Fig. 1A and B), SPR sensing of NH_3 using excitation wavelengths in the ~520 nm (the lowest wavelength accessible with gold [52]) to ~550 nm range will result in a blue-shift of the SPR dip, whereas at 560 nm and above, a red-shift will be registered. From the same figure it is also possible to predict that at ~550 nm, the presence of the analyte will not be registered since the refractive indeces of the two PAni forms overlap. Fig. 2 superimposes the difference in refractive index between the emeraldine salt and the emeraldine base with the response obtained to 192 ppm NH_3. Since a broadband light source was used for these studies, the coupling conditions were altered by changing the incident angle to yield the desired λ_{SPR}. As discussed, the performance of the sensor changes dramatically with the excitation wavelength. The same chemical stimulus can induce a 0.5 nm blue-shift and up to a 5 nm red-shift, with the potential of even higher shifts provided that longer wavelengths are accessible. The optical setup employed in these studies is restricted to an upper limit of ~640 nm, corresponding to the location of one of two Wood's anomalies (~520 nm and ~645 nm) displayed by the holographic grating (Horiba Scientific catalog no. 510 09 120). Convolution of the SPR band with the Wood's anomaly results in a distorted spectrum wherein the SPR dip minimum becomes obscured. At

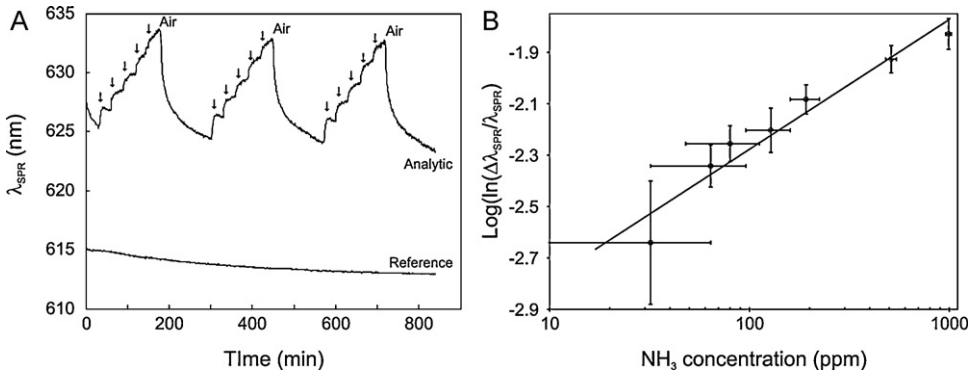

Fig. 3. (A) Calibration and reference sensorgram for five (32 ppm, 80 ppm, 192 ppm, 512 ppm and 992 ppm) of the seven NH_3 concentrations (64 ppm and 128 ppm are not shown) tested. (B) Linearized calibration ($N = 6$) for PAni-CSA SPR sensor. *Note*: Calibration of PAni-CSA sensor was performed in two separate measurement cycles. The number of spectra collected for each measurement cycle was limited due to the ability of the software interface to handle the number of data points generated. Including all seven NH_3 concentrations yielded exceedingly long computation times, oftentimes resulting in software instability.

wavelengths beyond the range of the Wood's anomaly, the SPR dip becomes too shallow due to the continuously increasing k of the polymer, and cannot be measured. Finally, the influence of gas-phase NH_3 on the SPR sensor was tested by measuring the λ_{SPR} shift obtained with bare gold slides, wherein the full evanescent wave is in direct contact with the analyte. In this case, exposure to 192 ppm NH_3 induced a red-shift of 0.08 ± 0.01 nm ($N = 3$), compared to 5.60 ± 0.22 nm ($N = 3$) for PAni-CSA coated sensors (at $\lambda_{SPR} = 640$ nm), indeed confirming that signal contributions from the portion of the plasmon wave protruding past the PAni-CSA layer and into the gas-phase are negligible.

Given the aforementioned optical constrains, calibration of the sensor and testing of the dynamic response was performed at $\lambda_{SPR} \sim 625$ nm, providing ~20 nm of range to cover the span of NH_3 concentrations tested (up to 992 ppm) without interferences from the Wood's anomaly. An exemplary sensorgram of PAni-CSA coated sensors to increasing ammonia concentrations is presented in Fig. 3A. The calibration was separated into two sets of concentrations; the first one comprised of 32 ppm, 80 ppm, 192 ppm, 512 ppm and 992 ppm NH_3, while the second completed the range with 64 ppm and 128 ppm NH_3. A single run with all seven concentrations resulted in matrices too large for the Horiba SynerJY software platform (v. 1.8.5.0) to reliably control collection of the spectra and format the data. Oftentimes this lead to software crashing and loss of data.

The electrical properties of emeraldine salts are related to NH_3 concentration following:

$$R = R_O \ \exp[(\alpha N)^{\gamma}] \quad (2)$$

where R and R_O correspond to the resistance measured in the presence and absence of the analyte, respectively, N is the NH_3 concentration in ppm and α and γ are constants [33]. The same equation can be adapted for optical measurements [53,54], where changes in absorbance at predefined wavelengths, rather than electrical resistivity, are quantified. The response of PAni-CSA coated SPR sensors to NH_3 appears similar, in that, generally speaking, a logarithmic response is obtained with increasing NH_3 content. If R_O and R in Eq. (2) are replaced by $\lambda(\text{air})_{SPR}$ and $\lambda(NH_3)_{SPR}$, respectively, the response can be linearized [33] as depicted in Fig. 3B.

Fig. 3B also shows that the error in determining the SPR shift associated with different NH_3 concentrations is comparatively constant (~3% of the measured value, $N = 6$) with the exception of 32 ppm, which displays markedly higher variance (~9%, $N = 6$) and leads to a modest mathematical fit (R^2 value of 0.943). The high error in measuring the shift displayed by the lowest concentration is most likely associated with the resolution of the MFCs utilized, which is ±1.5% of the full scale, or ±32 ppm NH_3, indicating that dilutions at the functional limits MFCs are unreliable. If the SPR shift at 32 ppm is not considered in the sensor calibration, the R^2 value of the fit improves substantially to 0.987. Extrapolation from the regression equation (including data acquired with 32 ppm NH_3) to a signal-to-noise ratio of 3 (based on standard deviation of the response to dry air at $\lambda_{SPR} \sim 625$ nm) indicates that a theoretical limit of detection (LOD) of ~0.2 ppm NH_3 may be achievable. This value represents an optimistic interpretation of the data, and it is likely that a truly experimental LOD would not match the levels predicted. Unfortunately, due to dilution limitations of the MFCs an experimental LOD cannot be determined. It is important to note that even if the experimental LOD is estimated to reach 10 ppm, 50× higher than the predicted value, it is still within typical ranges reported for NH_3 sensing platforms utilizing the emeraldine salt form of PAni [53–59]. Performing the analysis at longer wavelengths, thereby taking advantage of larger changes in n – which peaks at ~720 nm – may yield an improved LOD. However, it then becomes a balancing act between the shift λ_{SPR} recorded and the noise introduced by the continuously broadening, less prominent, SPR dip.

Finally, Fig. 3A also includes the response obtained from the reference channel. SPR spectroscopy is considered a zeroth order technique, whereby the signal measured is non-specific. Therefore, a reference channel consisting of a spectroscopically probed area adjacent to the analytic channel is included in the flow cell design. The reference channel is continuously flushed with the carrier gas (synthetic dry air) at 100 mL/min. Drift in the reference channel, which may rise from (for e.g.) temperature fluctuations, can then be used to compensate for drift in the analytic channel. Finally, although the effect of interferents on the sensor was not experimentally verified in this contribution, it has been demonstrated that doped PAni will respond to other analytes, including H_2O, CH_3OH, N_2H_4 and H_2, among others [30,60,61]. Therefore, measurements in complex matrices would benefit from a sensing array system, whereby each transducer is modified with different chemical recognition strategies [62,63].

The dynamic response of the PAni-CSA coating is commonly evaluated with respect to the τ_{90} value (the time required to attain 90% of the full signal). For the particular setup, despite an initial sharp rise in RI, the signal requires 6–7 min to achieve the τ_{90} value, which is longer than other techniques utilizing PAni (Fig. 4). Desorption of NH_3 from the polymer is delayed even further, requiring ~120 min to return to baseline values. Fig. 4 also shows the λ_{SPR} shift obtained with bare gold compared to PAni-CSA. Though averaging of five spectra results in a loss in temporal resolution

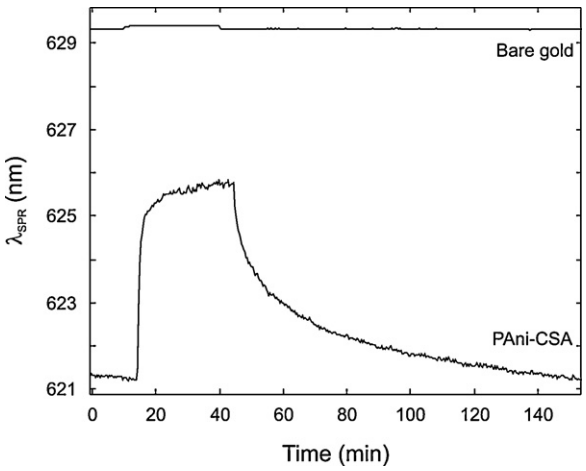

Fig. 4. Temporal response to 192 ppm NH_3 of bare and PAni-CSA coated SPR chips corrected for background drift.

compared to single spectrum acquisition, the slow response times of PAni-CSA to NH_3 suggests that little temporal information is truly lost.

A survey of recent literature contributions employing doped PAni layers of similar thicknesses (100–200 nm) indicates that the polymer usually responds to NH_3 adsorption within 1 min and returns to baseline in <10 min once the stimulus is removed [54,56,57]. These values are lower than those experienced here. Though the gas flow rates used (100 mL/min) are lower than those reported by most (up to 900 mL/min [56]), it is unlikely to be the cause for the delayed response/recovery since diffusion in- and out-of the polymer is the process responsible for the signal change [33,53]. Dopants used in PAni can influence the conductivity and permeability of the layers casted [64–68]. CSA has been used as a dopant in other NH_3 sensing platforms displaying shorter temporal responses [38,55,56], therefore dopant composition or doping levels are also unlikely to be the cause of the long response times observed here. Finally, it has been reported that the detection of NH_3 at trace levels (ppb) is challenging, as the analyte readily adheres to materials used in experimental setups [69–71], yielding hysteresis effects. Considering that analyte is delivered to the flow cell using ~2.5 m of 1/16″ (o.d.) stainless steel tubing, it is possible that sufficient surface area is available to retain the analyte at concentrations above the LOD (low to sub-ppm) of the SPR sensor. Ways of mitigating this effect include raising the gas flow-rate, gentle heating of the steel tubing and reducing the tubing length, will guide future efforts towards an improved temporal response.

4. Conclusion

Drop-casted polyaniline doped with camphorsulfonic acid (PAni-CSA) layers were evaluated with regards to their ability to sense gas-phase NH_3 using SPR spectroscopy. FT-IR and UV–Vis spectroscopy confirmed that the layers deposited correspond to the electrically conducting emeraldine salt form of the polymer. Measurement of the layer thickness by atomic force microscopy showed that the deposition procedure yields 160 nm thick layers, indicating that at longer wavelengths (>560 nm) the plasmon wave protrudes above the polymer and into the gas-phase. However, measurements performed with uncoated gold chips suggest that contributions from gas-phase detection of NH_3 are negligible compared to the response obtained with PAni-CSA. Spectroscopic ellipsometry was employed to extract both the real and imaginary components of the refractive index (n and k) for both the emeraldine salt and emeradine base. Comparison of the optical constants show that a wavelength-dependent response to NH_3 can be expected, corroborating observations with SPR spectroscopy. Finally, typical figures of merit with regards to NH_3 sensing showed that this approach is capable of achieving a limit of detection comparable to more established schemes, though with slower response times.

Acknowledgements

The authors would like to thank the American Heart Association (grant no. 09POST2120014) and the Delaware EPSCoR program (grant no. DBIO312214) for funding. Dr. I. Sasaki is acknowledged for helpful discussion pertaining preparation of PAni-CSA. Dr. S. Kohli from the Department of Chemistry at Colorado State University is acknowledged for collection and analysis of the ellipsometric data.

Appendix A. Supplementary data

Supplementary data associated with this article can be found, in the online version, at doi:10.1016/j.talanta.2011.06.020.

References

[1] J. Homola, Surface Plasmon Resonance Based Sensors, Springer, Berlin, 2006.
[2] R.B.M. Schasfoort, A.J. Tudos, Handbook of Surface Plasmon Resonance, Royal Society of Chemistry, Cambridge, 2008.
[3] R.J. Green, R.A. Frazier, K.M. Shakesheff, M.C. Davies, C.J. Roberts, S.J.B. Tendler, Biomaterials 21 (18) (2000) 1823–1835.
[4] C.T. Campbell, G. Kim, Biomaterials 28 (15) (2007) 2380–2392.
[5] T.M. Battaglia, J.F. Masson, M.R. Sierks, S.P. Beaudoin, J. Rogers, K.N. Foster, G.A. Holloway, K.S. Booksh, Anal. Chem. 77 (21) (2005) 7016–7023.
[6] O.R. Bolduc, J.N. Pelletier, J.-F. Masson, Anal. Chem. 82 (9) (2010) 3699–3706.
[7] J. Homola, Chem. Rev. 108 (2) (2008) 462–493.
[8] M.A. Cooper (Ed.), Label-Free Biosensors: Techniques and Applications, Cambridge University Press, Cambridge, 2009.
[9] A. Nooke, U. Beck, A. Hertwig, A. Krause, H. Krueger, V. Lohse, D. Negendank, J. Steinbach, Sens. Actuators B B149 (1) (2010) 194–198.
[10] A.B. El-Basaty, T.A. El-Brolossy, S. Abdalla, S. Negm, R.A. Abdella, H. Talaat, Surf. Interface Anal. 40 (13) (2008) 1623–1626.
[11] S.M. Aliwi, A.K. Hassan, Sens. Actuators B B133 (2) (2008) 521–525.
[12] T. Basova, E. Kol'tsov, A. Hassan, A. Tsargorodskaya, A. Ray, I. Igumenov, Phys. Status Solidi B 242 (4) (2005) 822–827.
[13] M.G. Manera, J. Spadavecchia, D. Buso, C. de Julian Fernandez, G. Mattei, A. Martucci, P. Mulvaney, J. Perez-Juste, R. Rella, L. Vasanelli, P. Mazzoldi, Sens. Actuators B B132 (1) (2008) 107–115.
[14] C. de Julian Fernandez, M.G. Manera, G. Pellegrini, M. Bersani, G. Mattei, R. Rella, L. Vasanelli, P. Mazzoldi, Sens. Actuators B B130 (1) (2008) 531–537.
[15] E. Maciak, Z. Opilski, T. Pustelny, A. Stolarczyk, Proc. SPIE-Int. Soc. Opt. Eng. 5956 (Integrated Optics: Theory and Applications) (2005), 59561K/59561–59561K/59569.
[16] D. Yang, H.-H. Lu, B. Chen, C.-W. Lin, Sens. Actuators B B145 (2) (2010) 832–838.
[17] Y.-D. Wang, Z.-X. Chen, Y.-F. Li, Z.-L. Zhou, X.-H. Wu, Solid-State Electron. 45 (5) (2001) 639–644.
[18] A. Katerkamp, P. Bolsmann, M. Niggemann, M. Pellmann, K. Cammann, Mikrochim. Acta 119 (1–2) (1995) 63–72.
[19] M.G. Manera, C. de Julian Fernandez, G. Maggioni, G. Mattei, S. Carturan, A. Quaranta, G. Della Mea, R. Rella, L. Vasanelli, P. Mazzoldi, Sens. Actuators B B120 (2) (2007) 712–718.
[20] S. Banerji, W. Peng, Y.-C. Kim, N. Menegazzo, K.S. Booksh, Sens. Actuators B B147 (1) (2010) 255–262.
[21] H. Bai, G. Shi, Sensors 7 (3) (2007) 267–307.
[22] J. Janata, M. Josowicz, J. Solid State Electrochem. 13 (1) (2009) 41–49.
[23] J. Janata, M. Josowicz, Nat. Mater. 2 (1) (2003) 19–24.
[24] D.W. Hatchett, M. Josowicz, Chem. Rev. 108 (2) (2008) 746–769.
[25] T. Hanawa, S. Kuwabata, H. Hashimoto, H. Yoneyama, Synth. Met. 30 (2) (1989) 173–181.
[26] T.A. Skotheim, R.L. Elsenbaumer, J.R. Reynolds (Eds.), Handbook of Conducting Polymers, 2nd ed., CRC Press, New York, 1997.
[27] N.E. Agbor, M.C. Petty, A.P. Monkman, Sens. Actuators B B28 (3) (1995) 173–179.
[28] N.E. Agbor, J.P. Cresswell, M.C. Petty, A.P. Monkman, Sens. Actuators B B41 (1–3) (1997) 137–141.
[29] A.V. Samoylov, V.M. Mirsky, Q. Hao, C. Swart, Y.M. Shirshov, O.S. Wolfbeis, Sens. Actuators B B106 (1) (2005) 369–372.
[30] G. Li, C. Martinez, J. Janata, J.A. Smith, M. Josowicz, S. Semancik, Electrochem. Solid-State Lett. 7 (10) (2004) H44–H47.
[31] H. Hu, M. Trejo, M.E. Nicho, J.M. Saniger, A. Garcia-Valenzuela, Sens. Actuators B B82 (1) (2002) 14–23.

[32] T.A. Skotheim, J.R. Reynolds, Handbook of Conducting Polymers, Third Edition: Conjugated Polymers, Theory, Synthesis, Properties, and Characterization, 3rd ed., CRC Press, Boca Raton, 2007.
[33] A.L. Kukla, Y.M. Shirshov, S.A. Piletsky, Sens. Actuators B B37 (3) (1996) 135–140.
[34] U. Lange, N.V. Roznyatovskaya, V.M. Mirsky, Anal. Chim. Acta 614 (1) (2008) 1–26.
[35] B. Timmer, W. Olthuis, A. van den Berg, Sens. Actuators B 107 (2) (2005) 666–677.
[36] A.J. Heber, J.-Q. Ni, T.T. Lim, P.-C. Tao, A.M. Schmidt, J.A. Koziel, D.B. Beasley, S.J. Hoff, R.E. Nicolai, L.D. Jacobson, Y. Zhang, J. Air Waste Manage. Assoc. 56 (10) (2006) 1472–1483.
[37] M.E. Webber, T. MacDonald, M.B. Pushkarsky, C.K. Patel, Y. Zhao, N. Marcillac, F.M. Mitloehner, Meas. Sci. Technol. 16 (8) (2005) 1547–1553.
[38] I. Sasaki, J. Janata, A. Glezer, IEEE Sens. J. 6 (6) (2006) 1728–1733.
[39] M. Trchova, J. Stejskal, J. Prokes, Synth. Met. 101 (1–3) (1999) 840–841.
[40] I. Sasaki, J. Janata, M. Josowicz, Polym. Degrad. Stab. 92 (7) (2007) 1408–1416.
[41] Y. Xia, J.M. Wiesinger, A.G. MacDiarmid, A.J. Epstein, Chem. Mater. 7 (3) (1995) 443–445.
[42] Y. Xia, A.G. MacDiarmid, A.J. Epstein, Macromolecules 27 (24) (1994) 7212–7214.
[43] D. Mo, Y.Y. Lin, J.H. Tan, Z.X. Yu, G.Z. Zhou, K.C. Gong, G.P. Zhang, X.F. He, Thin Solid Films 234 (1–2) (1993) 468–470.
[44] P. Kiattibutr, L. Tarachiwin, L. Ruangchuay, A. Sirivat, J. Schwank, React. Funct. Polym. 53 (1) (2002) 29–37.
[45] H.A. Al-Attar, A.D. Telfah, Opt. Commun. 229 (1–6) (2004) 263–270.
[46] H. Fujiwara, Spectroscopic Ellipsometry: Principles and Applications, John Wiley & Sons Ltd., Chichester, 2007.
[47] P.B. Johnson, R.W. Christy, B. Physical Review, Solid State 6 (12) (1972) 4370–4379.
[48] I. Pockrand, Surf. Sci. 72 (3) (1978) 577–588.
[49] S. Ekgasit, A. Tangcharoenbumrungsuk, F. Yu, A. Baba, W. Knoll, Sens. Actuators B B105 (2) (2005) 532–541.
[50] S. Ekgasit, C. Thammacharoen, F. Yu, W. Knoll, Anal. Chem. 76 (8) (2004) 2210–2219.
[51] I. Pockrand, J.D. Swalen, R. Santo, A. Brillante, M.R. Philpott, J. Chem. Phys. 69 (9) (1978) 4001–4011.
[52] C. Corti, R. Holliday (Eds.), Gold: Science and Application, CRC Press, Boca Raton, 2009.
[53] Z. Jin, Y.X. Su, Y.X. Duan, Sens. Actuators B 72 (1) (2001) 75–79.
[54] A. Airoudj, D. Debarnot, B. Beche, F. Poncin-Epaillard, Anal. Chim. Acta 626 (1) (2008) 44–52.
[55] A. Saheb, M. Josowicz, J. Janata, Anal. Chem. 80 (11) (2008) 4214–4219.
[56] D. Verma, V. Dutta, Sens. Actuators B B134 (2) (2008) 373–376.
[57] J. Chen, J. Yang, X. Yan, Q. Xue, Synth. Met. 160 (23–24) (2010) 2452–2458.
[58] K. Crowley, A. Morrin, A. Hernandez, E. O'Malley, P.G. Whitten, G.G. Wallace, M.R. Smyth, A.J. Killard, Talanta 77 (2) (2008) 710–717.
[59] M.E. Nicho, M. Trejo, A. Garcia-Valenzuela, J.M. Saniger, J. Palacios, H. Hu, Sens. Actuators B B76 (1–3) (2001) 18–24.
[60] M. Hirata, L. Sun, Sens. Actuators A 40 (2) (1994) 159–163.
[61] B.H. Weiller, S. Virji, J. Huang, R.B. Kaner, Polym. Prepr. 45 (1) (2004) 543–544.
[62] K.D. Shimizu, C.J. Stephenson, Curr. Opin. Cell Biol. 14 (6) (2010) 743–750.
[63] I. Sasaki, Higher-Order Sensors for Fast Detection of Gases, Department of Chemistry and Biochemistry, Georgia Institute of Technology, Atlanta, 2005, p. 93.
[64] S. Sinha, S. Bhadra, D. Khastgir, J. Appl. Polym. Sci. 112 (5) (2009) 3135–3140.
[65] K. Xu, L. Zhu, J. Li, H. Tang, Electrochim. Acta 52 (2) (2006) 723–727.
[66] P.P. Sengupta, P. Kar, B. Adhikari, Thin Solid Films 517 (13) (2009) 3770–3775.
[67] G. Anitha, E. Subramanian, Sens. Actuators B B92 (1–2) (2003) 49–59.
[68] A.G. MacDiarmid, A.J. Epstein, Synth. Met. 69 (1–3) (1995) 85–92.
[69] M.A. Owens, C.C. Davis, R.R. Dickerson, Anal. Chem. 71 (7) (1999) 1391–1399.
[70] A. Schmohl, A. Miklos, P. Hess, Appl. Opt. 40 (15) (2001) 2571–2578.
[71] J.P. Besson, S. Schilt, E. Rochat, L. Thevenaz, Appl. Phys. B: Lasers Opt. 85 (2–3) (2006) 323–328.